Applied Physics Letters

Electronic and magnetic properties of quasi-one-dimensional osmium halide $OsCl_4$

Cite as: Appl. Phys. Lett. **120**, 023101 (2022); https://doi.org/10.1063/5.0079570
Submitted: 22 November 2021 • Accepted: 27 December 2021 • Published Online: 10 January 2022

Yang Zhang, Ling-Fang Lin, Adriana Moreo, et al.

COLLECTIONS

Paper published as part of the special topic on One-Dimensional van der Waals Materials

Applied Physics Letters ARTICLE scitation.org/journal/apl

Electronic and magnetic properties of quasi-one-dimensional osmium halide $OsCl_4$

Cite as: Appl. Phys. Lett. **120**, 023101 (2022); doi: 10.1063/5.0079570
Submitted: 22 November 2021 · Accepted: 27 December 2021 ·
Published Online: 10 January 2022

Yang Zhang,[1,a)] Ling-Fang Lin,[1] Adriana Moreo,[1,2] and Elbio Dagotto[1,2]

AFFILIATIONS

[1]Department of Physics and Astronomy, University of Tennessee, Knoxville, Tennessee 37996, USA
[2]Materials Science and Technology Division, Oak Ridge National Laboratory, Oak Ridge, Tennessee 37831, USA

Note: This paper is part of the APL Special Collection on One-Dimensional van der Waals Materials.
[a)]**Author to whom correspondence should be addressed:** yzhang@utk.edu

ABSTRACT

Using *ab initio* density functional theory, we study the electronic and magnetic properties of the van der Waals chain material $OsCl_4$. In the nonmagnetic state, a strongly anisotropic band structure was observed, in agreement with its anticipated one-dimensional crystal geometry. Based on Wannier functions, we found that the four electrons of the $5d$ Os atom form a low-spin $S = 1$ state, with a large crystal field between the $d_{xz/yz}$ and d_{xy} orbitals, corresponding to a strong Jahn–Teller distortion ($Q_3 < 0$). As a consequence, the magnetic properties are mainly contributed by the $d_{xz/yz}$ states. Furthermore, when a Mott gap develops after the introduction of the Hubbard U and Hund coupling J, we found that the staggered spin order is the most likely magnetic state, namely, spins arranged as (↑-↓-↑-↓) with π wavevector along the chain. In addition, the energy differences between various spin states are small, suggesting a weak magnetic exchange coupling along the chain. Our results provide guidance to experimentalists and theorists working on quasi-one-dimensional osmium halides chain materials.

Over several decades, one-dimensional (1D) systems have attracted considerable attention due to their interesting physical properties.[1–3] In these 1D systems, remarkable physical phenomena have been found or predicted, such as high-T_c superconductivity in iron or copper chains and ladders,[4–10] exotic insulating ferromagnetism in a 1D iron oxychalcogenide,[11] ferroelectricity triggered by phonon modes or spin ordering,[12–16] charge density wave or spin density wave states due to the partial or complete condensation of excitations of free carriers,[2,3,17,18] spin block states in the orbital-selective Mott regime of iron 1D ladders or chains,[15,19–21] and several others. In general, the spin–orbit coupling (SOC) λ is considered to be negligible for 1D systems with $3d$ transition-metal (TM) atoms, where their physical properties are primarily induced by electronic correlation couplings (i.e., Hubbard repulsion U and Hund coupling J_H).

However, the strength of the SOC parameter λ is enhanced in $4d/5d$ TM atoms[22] leading to comparable values between λ, U, and J_H, resulting in several intriguing electronic phases. For example, if the intrahopping t is larger than the typical Hund coupling, an interesting orbital-selective Peierls phase was found in some 1D dimer systems with $4d^2$ or $5d^2$ electronic configurations, where the localized band is induced by a Peierls distortion.[23,24]

Because of a reduced J_H, $4d/5d$ atoms often favor the low-spin configuration in compounds with more than half-filled t_{2g} orbitals. Under a cubic crystal field, the five d orbitals split into the lower t_{2g} and higher e_g bands separated by a crystal-field splitting energy (∼10 Dq). Then, by introducing the SOC effect, the $J_{\rm eff} = 1/2$ and $J_{\rm eff} = 3/2$ states separate from each other [see Fig. 1(a)]. However, in these $4d^5$ or $5d^5$ systems, the Hubbard repulsion U can dramatically modify the electronic distribution and induce the localization of the spin–orbit coupled pseudospin degree of freedom, leading to half-occupied $J_{\rm eff} = 1/2$ "spin–orbit Mott" insulating states.[25,26] For the d^4 electronic configurations, such as Ru^{4+}, Os^{4+}, and Ir^{5+}, all four electrons occupy three degenerate t_{2g} orbitals under a cubic crystal field, leading to a total spin $S = 1$ and orbital moment $L = 1$. Returning to the case $U = 0$, including SOC with $\lambda > 0$, this d^4 system is expected to be a nonmagnetic (NM) insulator of local two-hole $J = 0$ singlets.[27,28] By considering mobile spin–orbital excitons, their condensation may lead to a magnetically ordered state according to theoretical studies.[27–32] However, some real materials with d^4 electronic configuration have displayed magnetism at low temperature, instead of the nonmagnetic insulator of $J = 0$ singlets, such as the double perovskite iridates Sr_2YIrO_6[33] and Ba_2YIrO_6.[34] One theoretical calculation suggests that band structure effects induce the breakdown of the $J = 0$ singlet state dominance because the noncubic crystal-field effect is quite small in these compounds.[35]

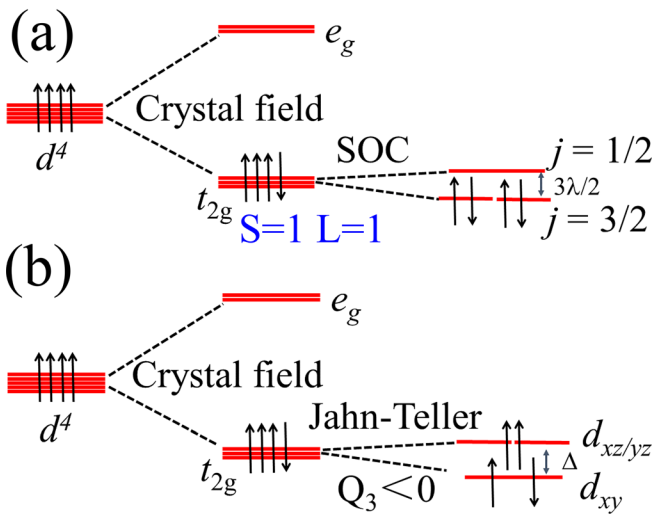

FIG. 1. (a) Schematic energy splitting of the d^4 low-spin configuration with strong SOC under a cubic crystal field. (b) Schematic energy splitting of the d^4 low-spin configuration under a Jahn–Teller distortion ($Q_3 < 0$).

The Jahn–Teller (JT) Q_3 distortion is a common phenomenon in real materials, which would also cause the energy splitting of t_{2g} orbitals. As displayed in Fig. 1(b), the JT distortion could induce the splitting of the three degenerate t_{2g} orbitals into a two upper degenerate d_{xz} and d_{yz} states, separated from d_{xy} by the crystal-field splitting energy (Δ) when $Q_3 < 0$. If λ is large enough, the strong SOC could fully suppress the JT distortion, leading again to a stable $J = 0$ singlet in the d^4 configuration system.[36] Previous studies have mainly focused on three-dimensional or layered materials for the $4d/5d$ systems with the d^4 electronic configurations. Due to the reduced dimensional phase space, the JT Q_3 distortion is expected to be large in some 1D or quasi-1D vdW systems.[12,24] Hence, this naturally introduces a simple question: is there any real 1D material with d^4 configurations having strong JT distortion and SOC effects?

In this Letter, we use first-principles density functional theory (DFT) method with the generalized gradient approximation (GGA)[37–40] to investigate the 1D vdW chain system $OsCl_4$. Our results are summarized as follows. First, the *ab initio* DFT calculations indicate a strongly anisotropic electronic band structure for $OsCl_4$, in agreement with its anticipated 1D crystal geometry. Based on the Wannier functions resulting from first-principles calculations, we obtained the relevant hopping amplitudes and the crystal-field splitting energy of the t_{2g} orbitals for the Os atoms. Because of the large crystal-field splitting energy between $d_{xz/yz}$ and d_{xy}, $OsCl_4$ with the d^4 configuration is a spin-1 $S = 1$ system, instead of a $J = 0$ singlet ground state. Furthermore, the superexchange Hubbard interaction is dominant, leading to a Mott antiferromagnetic (AFM) state in the chain direction. In addition, our DFT calculations suggest that the staggered spin order with wavevector π (↑-↓-↑-↓) is the most likely magnetic ground state along the chain.

As shown in Fig. 2(a), $OsCl_4$ has an orthorhombic crystal structure with space group Cmmm (No. 65),[41] where the $OsCl_6$ octahedra form edge-sharing vdW 1D chains along the c-axis. Under ambient conditions, based on experiments,[41] the nearest neighbor (NN) Os–Os

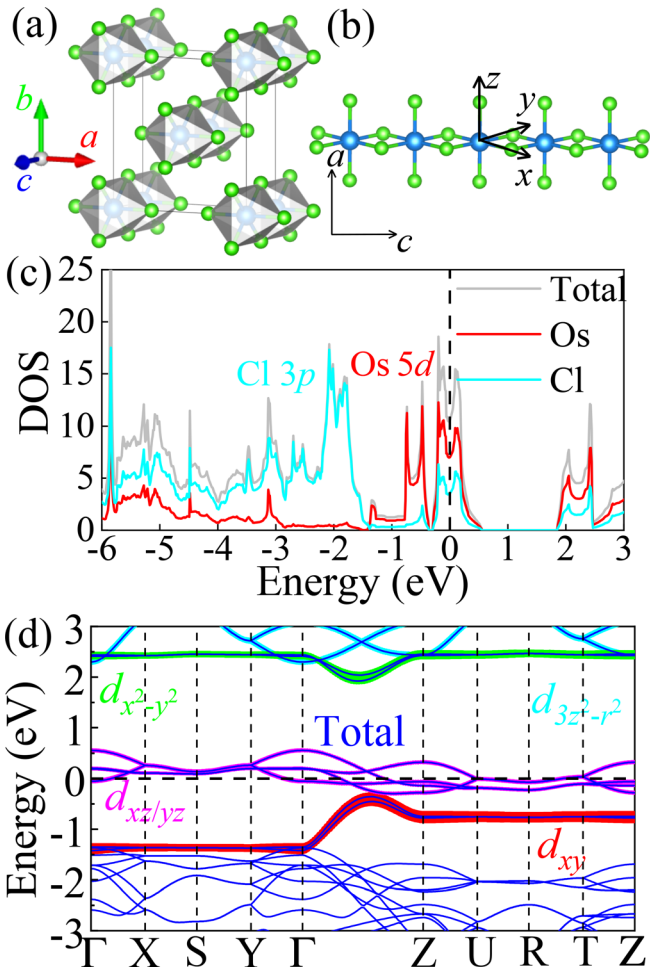

FIG. 2. (a) Schematic crystal structure of the conventional cell of $OsCl_4$ drawn by VESTA[42] with the convention: blue = Os and green = Cl. (b) The crystal structure showing the Os–Cl–Os chain direction. The angles of the Cl–Os–Cl and Os–Cl–Os bonds are 83.08° and 96.92°, respectively. (c) DOS near the Fermi level based on the nonmagnetic states for $OsCl_4$. Gray: total; red: Os; cyan: Cl. (d) Projected band structures of $OsCl_4$ in the nonmagnetic state without SOC. The d_{xy} orbital is on the b–c plane, with the x- or y-axis along the Os–Cl directions, while the z-axis is along the a-axis. The Fermi level is shown with dashed horizontal lines. Each osmium orbital is represented by lines of different colors. The coordinates of the high-symmetry points in the bulk Brillouin zone (BZ) are Γ = (0, 0, 0), X = (0.5, 0, 0), S = (0.5, 0.5, 0), Y = (0, 0.5, 0), Z = (0, 0, 0.5), U = (0.5, 0, 0.5), R = (0.5, 0.5, 0.5), and T = (0, 0.5, 0.5).

distances ($d_{Os-Os} = 3.56$ Å) are identical along each chain. In those chains, the system has four identical Os–Cl bonds (~2.378 Å) in the b–c plane and two short Os–Cl bonds (~2.261 Å) along the a axis, resulting in a Jahn–Teller distortion $Q_3 < 0$. In this case, the three degenerate t_{2g} orbitals split into two higher energy levels (d_{xz} and d_{yz}) and one lower energy level (d_{xy}). Considering the location of Os in the periodic table, the SOC effect should be large in $OsCl_4$. Due to the compression of the $OsCl_6$ octahedra, this system forms an effective $S = 1$ low-energy state if the crystal-field splitting Δ between $d_{xz/yz}$ and d_{xy} is sufficiently large.

Let us now discuss the electronic structure of $OsCl_4$ in the nonmagnetic (NM) phase without SOC. According to the calculated density of states (DOS), the states near the Fermi level are mainly contributed by the Os-5d t_{2g} orbitals, hybridized with some Cl-3p orbitals [see Fig. 2(c)]. Most states related to the Cl-3p orbitals are away from the Fermi level, located in the energy range from -6 to -1.5 eV. In this case, the charge transfer gap $\Delta = \varepsilon_d - \varepsilon_p$ is large, indicating that $OsCl_4$ is a Mott–Hubbard system rather than a charge-transfer system.

As shown in Fig. 2(d), $OsCl_4$ displays a strongly quasi-1D electronic behavior near the Fermi level along the c-axis corresponding to its dominant chain geometry, where the band structure is much more dispersive along that axis (Γ-Z path) than other directions. Based on the projected band structures of Os's 5d orbitals, the e_g orbitals ($d_{x^2-y^2}$ and $d_{3z^2-r^2}$) are located at high-energy bands above the Fermi level and, thus, unoccupied, in agreement with the analysis of the low-spin configuration with Os^{4+} valence and d^4 configuration. Furthermore, two 5d electrons of Os occupy the d_{xy} state with flatband characteristics except the Γ–Z path because the d_{xy} orbital is lying in the b–c plane. The other two 5d electrons of Os occupy the d_{xz} and d_{yz} orbitals. Consequently, this system can be accurately regarded as having four electrons per site on three t_{2g} orbitals. Based on the band structure information, the magnetic properties of $OsCl_4$ are contributed by the two electrons on the d_{xz} and d_{yz} orbitals.

Figure 3(a) shows that the bands begin to split after introducing the SOC to $OsCl_4$, opening an energy gap (~0.16 eV) above the Fermi level at the Γ point for the $d_{xz/yz}$ bands. In addition, we also considered the electronic correlations ($U = 2$ eV and $J = 0.4$ eV) on the Os sites, in a screened Hartree–Fock-like manner, as in the local density approximation (LDA) + U method with Liechtenstein format within the double-counting item.[43] The lower-energy bands of the fully occupied d_{xy} orbital begin to shift away of the Fermi level under the influence of the electronic correlations. To better understand the low-energy bands of $OsCl_4$, we constructed the disentangled Wannier function of those low-energy bands in the NM phase without SOC, based on the maximally localized Wannier method.[44] As shown in Figs. 3(b)–3(d), those orbitals display clearly d_{xz}, d_{yz}, and d_{xy} characteristics. Based on the Wannier function basis (d_{xz}, d_{yz}, d_{xy}), here referred to as $\gamma = (0, 1, 2)$, respectively, we also obtained the NN hopping matrix for the NN two Os sites in the chain direction,

$$t_{\gamma\gamma'} = \begin{bmatrix} 0.064 & -0.029 & 0.000 \\ -0.029 & 0.070 & 0.000 \\ 0.000 & 0.000 & -0.134 \end{bmatrix}. \quad (1)$$

All the hopping matrix elements are in eV units. The crystal-field splitting Δ between $d_{xz/yz}$ and d_{xy} orbitals is about -0.721 eV, caused by the JT distortion Q_3. (Additional Wannier results can be found in the supplementary material.) Note that the angle formed by Os–Cl–Os is not 90°, leading to the local y-axis to be not strictly pointing along the Os–Cl bond, resulting in a small difference of hopping values between the d_{xz} and d_{yz} orbitals.

Because Δ is larger than J_H and λ, this system would form stable $S = 1$ states with one fully occupied d_{xy} orbital and two half-occupied $d_{xz/yz}$ orbitals, instead of the expected $J = 0$ singlet state in the $5d^4$ configuration. Based on our previous second-order perturbation theory analysis and density matrix renormalization group (DMRG) calculations, large entanglements between doubly occupied and half-filled orbitals can play a key role in stabilizing FM order in a 1D model (three electrons in four orbitals).[11] However, the hopping between the doubly occupied d_{xy} and the half-filled $d_{xz/yz}$ orbitals is forbidden in $OsCl_4$. Then, the magnetic properties of this system are mainly decided by the $d_{xz/yz}$ orbitals. Due to the Pauli principle, the two NN sites favor AFM exchange coupling in the chain direction, as shown in Fig. 3(e). Hence, the superexchange Hubbard interaction is dominant, leading to a robust staggered AFM state. In this case, intuitively, the most likely magnetic ordering is AFM, i.e., (↑-↓-↑-↓). Furthermore, considering the values of the hopping amplitudes of the $d_{xz/yz}$ orbitals, this system should be easily localized after introducing the Hubbard interaction U.

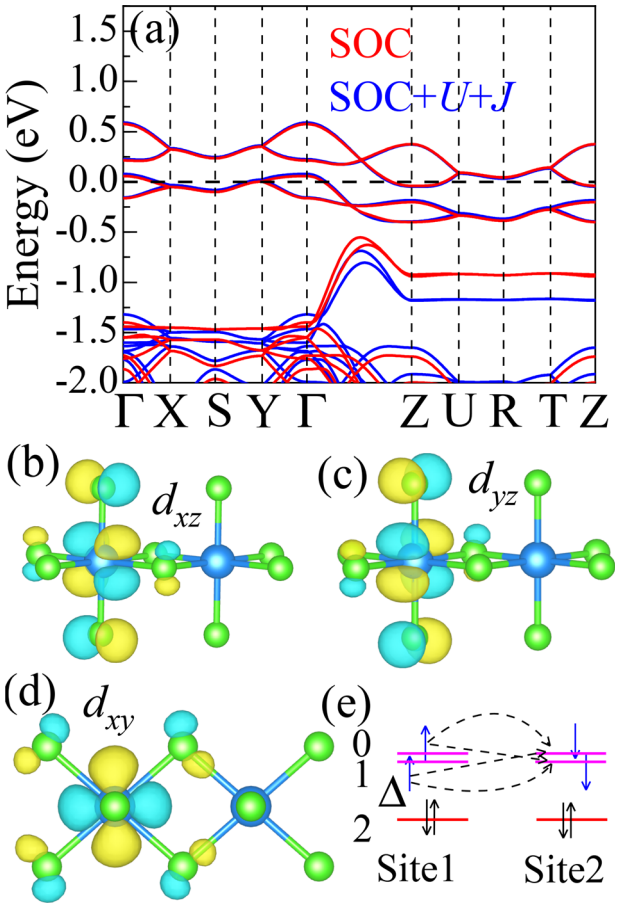

FIG. 3. (a) Band structure of $OsCl_4$ in the nonmagnetic state with SOC and with SOC + U + J ($U = 2$ eV, $J = 0.4$ eV). The Fermi level is the horizontal dashed line. (b)–(d) Wannier function of the three Os t_{2g} orbitals, with lobes of opposite signs colored as blue and yellow: (b) d_{xz}, (c) d_{yz}, (d) d_{xy}. Os and Cl atoms are in blue and green, respectively. (e) AFM superexchange path for two NN sites.

To confirm our intuitive analysis, we used the LDA + U method[43] to compare different spin configurations along the chain of $OsCl_4$ by changing the onsite Coulomb interaction U and onsite exchange interaction J. Here, we considered AFM1 (↑-↓), AFM2 (↑-↑-↓-↓), AFM3 (↑-↑-↑-↓-↓-↓), AFM4 (↑-↑-↑-↑-↓-↓-↓-↓), FM, and

NM configurations along the chain direction, while the magnetic coupling between NN chain is regarded as FM. (Detail can be found in the supplementary material.)

Based on the experimental crystal structure,[41] using periodic boundary conditions, with DFT, we constructed the phase diagram of the 1D chain present in $OsCl_4$ with electronic density $n = 4$. As shown in Fig. 4(a), there is only one AFM magnetic state (specifically, AFM1) stable in our DFT phase diagram, supporting our intuitive analysis. Note that we compared the energies of the several different magnetic configurations mentioned before, with or without SOC, and obtained the same results. This DFT phase diagram is in agreement with our previous DMRG study on the 1D chain model with three electrons in four orbitals, where the diagonal intraorbital hopping is dominant.[16] Furthermore, we also observed a metal–insulator phase transition at $U = 1$ eV. Because the hopping terms are not too large, the effects of the Hubbard U occur at this relatively small value. Note that the location of the boundary between the metal and the insulator should be considered only as a crude approximation. However, the NM–AFM1 and metallic–insulator phase transitions are clearly established, by considering the physical effects of hoppings and electronic correlations.

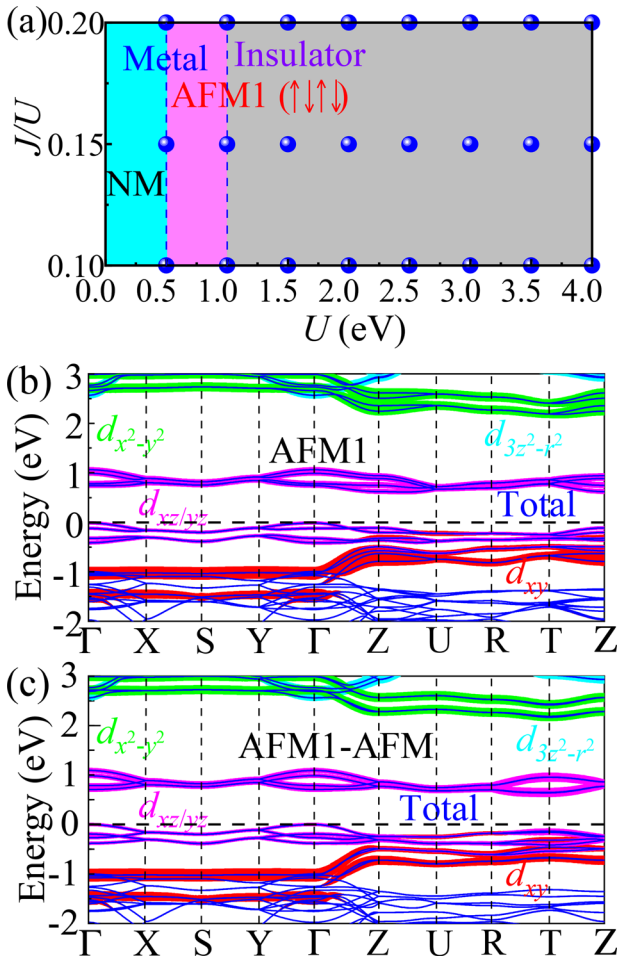

FIG. 4. (a) Phase diagram based on the experimental lattice constants of $OsCl_4$, employing the LDA + U technique with the electronic density $n = 4$. Small solid circles indicate the specific values that were investigated with DFT calculations. (b) and (c) Projected band structures of $OsCl_4$ for the AFM1 state with SOC for different inter-chain couplings: (b) AFM1 (FM coupling between chains) and (c) AFM1–AFM (AFM coupling between chains). The Fermi level is the horizontal dashed line.

Next, we also relaxed the crystal structures for the spin configurations mentioned before based on the LDA + U method with Liechtenstein format.[43] Both the lattice constants and atomic positions were fully relaxed with vdW interactions within zero damping vdW-D3.[45] Note that the vdW interactions mainly affect the lattice constants between chains but do not change the results of magnetic properties. Based on previous experimental and theoretical studies for 5d Ir or Os compounds,[46–48] U is in the range 1–3 eV and J in the range 0.3–0.5 eV. Consequently, here, we used the averages $U = 2$ eV and $J = 0.4$ eV as the appropriate values for the Os atoms.[22,48]

Then, we compared the energies of those different spin configurations based on the optimized structures with or without SOC effect, as listed in Table I. The AFM1 magnetic order always has the lowest energy among all tested candidates, with or without SOC. Furthermore, all the energy differences between different spin states are small, suggesting a weak magnetic exchange coupling along the chain direction, in agreement with our previous intuitive analysis from the results of Wannier functions. Based on the difference of energy between the AFM1 and FM states, we obtained that the NN Heisenberg magnetic exchange couplings are 9.85 and 5.85 meV for the GGA + U and GGA + U + SOC calculations, respectively, suggesting that the magnetic transition temperature must be low. For the AFM1 phase without SOC, the calculated local spin magnetic moment of Os is about 1.3 μ_B/Os, corresponding to the low-spin $S = 1$ configuration in Os^{4+}. Upon turning on the SOC, the spin quantization axis pointed along the x-axis but with only a tiny difference in energy with respect to the y-axis, indicating the spin favors lying in the xy plane, corresponding to the b–c crystal plane. The calculated orbital moment is about 0.1 μ_B/Os. As shown in Fig. 4(b), we also calculated the band structure of the AFM1 phase of $OsCl_4$ with GGA + U + SOC ($U = 2$ eV, $J = 0.4$ eV). The half-occupied $d_{xz/yz}$ orbitals display Mott-insulating behavior with a gap ~0.7 eV, while the d_{xy} orbital has fully occupied behavior.

Finally, we calculated the AFM coupling between chains for the AFM1 configuration. We obtained the optimized crystal lattices ($a = 8.070$ Å, $b = 8.428$ Å, and $c = 3.601$ Å) for the case of AFM inter-chain order, which are close to the values for the AFM1 with FM inter-chain order. However, the energy of the AFM1-AFM state is lower by about 1 meV than the AFM1 state, suggesting that the coupling between chains is AFM. The calculated local spin magnetic moments of Os are about 1.31 μ_B/Os and 1.28 μ_B/Os for the GGA + U and GGA + U + SOC calculations. In addition, we also calculated the band structure of the AFM1-AFM phase with GGA + U + SOC, which is similar to the band structure of AFM1. More results can be found in the supplementary material.

In summary, we systematically studied the vdW 1D chain compound $OsCl_4$ by using first-principles DFT calculations. A strongly anisotropic 1D electronic band structure near the Fermi surface was observed in the NM state, in agreement with its dominant chain geometry. Based on the Wannier functions calculated from DFT, we obtained the NN hopping amplitudes and on-site energies for the Os

TABLE I. The optimized lattice constants (Å), energy differences (meV/Os) with respect to the AFM1 configuration taken as the reference of energy, and magnetic moment (μ_B/Os), for the various magnetic configurations here used. The experimental values (Exp. for short) are also listed for comparison. E(GGA + U) and E(GGA + U + SOC) indicate the calculated energies for different magnetic configurations without or with the SOC effect, respectively. The spin and orbital moments are distinguished by the symbols M_S and M_L. Note that there are two/three/four Os atoms along the c-axis in their minimum unit cell for the AFM2, AFM3, and AFM4 states, respectively, leading to the different lattice constants of c in those spin configurations.

	AFM1	AFM2	AFM3	AFM4	FM	NM	Exp.[41]
a	8.072	8.072	8.065	8.066	8.066	8.125	7.929
b	8.391	8.428	8.441	8.442	8.449	8.055	8.326
c	3.600	7.207	10.813	14.421	3.614	3.558	3.560
E (GGA + U)	1.296	1.310	1.320	1.300	1.342	0	⋯
E (GGA + U + SOC)	0.0	2.5	4.1	5.9	11.7	259.5	⋯
M_S (GGA + U + SOC)	1.267	1.278	1.285	1.291	1.300	0	⋯
M_L (GGA + U + SOC)	0.099	0.101	0.102	0.102	0.103	0	⋯

atoms. A spin $S = 1$ for the d^4 electronic configuration was observed due to the large crystal-field splitting energy of the t_{2g} orbitals. As a consequence, intuitively, the AFM1 state is expected to be the most likely ground state along the 1D chain direction (↑-↓-↑-↓). This staggered AFM order with π vector was found in our study in a robust portion of the DFT phase diagram at many values of U and J/U, based on the experimental crystal structure of $OsCl_4$. In addition, we also relaxed the crystal structures with the different magnetic configurations using LDA + U ($U = 2$ eV and $J = 0.4$ eV). The AFM1 magnetic order with a Mott gap always has the lowest energy among all tested candidates, with or without SOC. The small energy differences between different magnetic configurations suggest a small Heisenberg magnetic exchange coupling along the chain direction and a low magnetic transition temperature. We believe our results could encourage additional detailed experimental studies of quasi-1D osmium halide chain materials. With the help of crystal growers, measurements of the temperature dependence of the susceptibility as well as neutron scattering experiments could confirm our predictions.

See the supplementary material for additional theoretical results corresponding to $OsCl_4$, including calculation method, Wannier fitting, bandgaps, magnetic moments, and electronic structures.

The work of Y.Z., L.-F.L., A.M., and E.D. was supported by the U.S. Department of Energy (DOE), Office of Science, Basic Energy Sciences (BES), Materials Sciences, and Engineering Division.

AUTHOR DECLARATIONS

Conflict of Interest

The authors have no conflicts to disclose.

DATA AVAILABILITY

The data that support the findings reported in this study are available from the corresponding author upon request.

REFERENCES

[1] E. Dagotto, Rev. Mod. Phys. **66**, 763 (1994).
[2] G. Grüner, *Density Waves in Solids* (Perseus, Cambridge, MA, 2000).
[3] P. Monceau, Adv. Phys. **61**, 325 (2012).
[4] H. Takahashi, A. Sugimoto, Y. Nambu, T. Yamauchi, Y. Hirata, T. Kawakami, M. Avdeev, K. Matsubayashi, F. Du, C. Kawashima, H. Soeda, S. Nakano, Y. Uwatoko, Y. Ueda, T. J. Sato, and K. Ohgushi, Nat. Mater. **14**, 1008 (2015).
[5] Y. Zhang, L. F. Lin, J. J. Zhang, E. Dagotto, and S. Dong, Phys. Rev. B **95**, 115154 (2017).
[6] J.-J. Ying, H. C. Lei, C. Petrovic, Y.-M. Xiao, and V.-V. Struzhkin, Phys. Rev. B **95**, 241109(R) (2017).
[7] Y. Zhang, L. F. Lin, J. J. Zhang, E. Dagotto, and S. Dong, Phys. Rev. B **97**, 045119 (2018).
[8] Y. Zhang, L. F. Lin, A. Moreo, S. Dong, and E. Dagotto, Phys. Rev. B **100**, 184419 (2019).
[9] E. Dagotto and T. M. Rice, Science **271**, 618 (1996).
[10] M. Uehara, T. Nagata, J. Akimitsu, H. Takahashi, N. Mori, and K. Kinoshita, J. Phys. Soc. Jpn. **65**, 2764 (1996).
[11] L. F. Lin, Y. Zhang, G. Alvarez, A. Moreo, and E. Dagotto, Phys. Rev. Lett. **127**, 077204 (2021).
[12] L. F. Lin, Y. Zhang, A. Moreo, E. Dagotto, and S. Dong, Phys. Rev. Mater. **3**, 111401(R) (2019).
[13] L. F. Lin, Y. Zhang, A. Moreo, E. Dagotto, and S. Dong, Phys. Rev. Lett. **123**, 067601 (2019).
[14] C. Yang, M. Chen, S. Li, X. Zhang, C. Hua, C. Xiao, S. A. Yang, P. He, Z.-A. Xu, and Y. Lu, ACS Appl. Mater. Interfaces **13**, 13517 (2021).
[15] Y. Zhang, L. F. Lin, A. Moreo, S. Dong, and E. Dagotto, Phys. Rev. B **101**, 144417 (2020).
[16] Y. Zhang, L. F. Lin, A. Moreo, G. Alvarez, and E. Dagotto, Phys. Rev. B **103**, L121114 (2021).
[17] J. Gooth, B. Bradlyn, S. Honnali, C. Schindler, N. Kumar, J. Noky, Y. Qi, C. Shekhar, Y. Sun, Z. Wang, B. A. Bernevig, and C. Felser, Nature **575**, 315 (2019).
[18] Y. Zhang, L.-F. Lin, A. Moreo, S. Dong, and E. Dagotto, Phys. Rev. B **101**, 174106 (2020).
[19] J. Herbrych, J. Heverhagen, N. Patel, G. Alvarez, M. Daghofer, A. Moreo, and E. Dagotto, Phys. Rev. Lett. **123**, 027203 (2019).
[20] J. Herbrych, J. Heverhagen, N. Patel, G. Alvarez, M. Daghofer, A. Moreo, and E. Dagotto, Proc. Natl. Acad. Sci. U. S. A. **117**, 16226 (2020).
[21] Y. Zhang, L.-F. Lin, G. Alvarez, A. Moreo, and E. Dagotto, Phys. Rev. B **104**, 125122 (2021).
[22] W. Witczak-Krempa, G. Chen, Y. B. Kim, and L. Balents, Annu. Rev. Condens. Matter Phys. **5**, 57 (2014).
[23] S. V. Streltsov and D. I. Khomskii, Phys. Rev. B **89**, 161112(R) (2014).
[24] Y. Zhang, L. F. Lin, A. Moreo, and E. Dagotto, Phys. Rev. B **104**, L060102 (2021).
[25] B. J. Kim, H. Jin, S. J. Moon, J.-Y. Kim, B.-G. Park, C. S. Leem, J. Yu, T. W. Noh, C. Kim, S.-J. Oh, J.-H. Park, V. Durairaj, G. Cao, and E. Rotenberg, Phys. Rev. Lett. **101**, 076402 (2008).
[26] C. Lu and J.-M. Liu, Adv. Mater. **32**, 1904508 (2020).
[27] G. Khaliullin, Phys. Rev. Lett. **111**, 197201 (2013).

[28]O. N. Meetei, W. S. Cole, M. Randeria, and N. Trivedi, Phys. Rev. B **91**, 054412 (2015).
[29]C. Svoboda, M. Randeria, and N. Trivedi, Phys. Rev. B **95**, 014409 (2017).
[30]N. Kaushal, J. Herbrych, A. Nocera, G. Alvarez, A. Moreo, F. A. Reboredo, and E. Dagotto, Phys. Rev. B **96**, 155111 (2017).
[31]A. J. Kim, H. O. Jeschke, P. Werner, and R. Valentí, Phys. Rev. Lett. **118**, 086401 (2017).
[32]N. Kaushal, R. Soni, A. Nocera, G. Alvarez, and E. Dagotto, Phys. Rev. B **101**, 245147 (2020).
[33]G. Cao, T. F. Qi, L. Li, J. Terzic, S. J. Yuan, L. E. DeLong, G. Murthy, and R. K. Kaul, Phys. Rev. Lett. **112**, 056402 (2014).
[34]J. Terzic, H. Zheng, F. Ye, H. D. Zhao, P. Schlottmann, L. E. De Long, S. J. Yuan, and G. Cao, Phys. Rev. B **96**, 064436 (2017).
[35]S. Bhowal, S. Baidya, I. Dasgupta, and T. S. Dasgupta, Phys. Rev. B **92**, 121113 (2015).
[36]S. V. Streltsov and D. I. Khomskii, Phys. Rev. X **10**, 031043 (2020).
[37]G. Kresse and J. Hafner, Phys. Rev. B **47**, 558 (1993).
[38]G. Kresse and J. Furthmüller, Phys. Rev. B **54**, 11169 (1996).
[39]P. E. Blöchl, Phys. Rev. B **50**, 17953 (1994).
[40]J. P. Perdew, K. Burke, and M. Ernzerhof, Phys. Rev. Lett. **77**, 3865 (1996).
[41]F. A. Cotton and C. E. Rice, Inorg. Chem. **16**, 1865 (1977).
[42]K. Momma and F. Izumi, J. Appl. Crystallogr. **44**, 1272 (2011).
[43]A. Liechtenstein, V. Anisimov, and J. Zaanen, Phys. Rev. B **52**, R5467 (1995).
[44]A. A. Mostofi, J. R. Yates, Y. S. Lee, I. Souza, D. Vanderbilt, and N. Marzari, Comput. Phys. Commun. **178**, 685 (2008).
[45]S. Grimme, J. Antony, S. Ehrlich, and S. Krieg, J. Chem. Phys. **132**, 154104 (2010).
[46]B. Yuan, J. P. Clancy, A. M. Cook, C. M. Thompson, J. Greedan, G. Cao, B. C. Jeon, T. W. Noh, M. H. Upton, D. Casa, T. Gog, A. Paramekanti, and Y.-J. Kim, Phys. Rev. B **95**, 235114 (2017).
[47]E. Şaşioğlu, C. Friedrich, and S. Blügel, Phys. Rev. B **83**, 12101(R) (2011).
[48]Y. Du, X. Wan, L. Sheng, J. Dong, and S. Y. Savrasov, Phys. Rev. B **85**, 174424 (2012).